Synthesis and Characterization of Iron Doped Hydroxyapatite for Defluoridation of Water and Antibacterial Activity

Abebe Awulew Temtime
Adama Science and Technology University
Enyew Amare Zereffa (enyewama@yahoo.com)
Adama Science and Technology University
Dereje Tsegaye Leku
Adama Science and Technology University

Research Article

Keywords: Hydroxyapatite, Fe doped HAp, antibacterial activity, defluoridation, adsorbent

Posted Date: October 7th, 2022

DOI: https://doi.org/10.21203/rs.3.rs-2123671/v1

Synthesis and Characterization of Iron Doped Hydroxyapatite for Defluoridation of Water and Antibacterial Activity

Abebe Awulew Temtime, Enyew Amare Zereffa, Dereje Tsegaye Leku

Department of Applied Chemistry, School of Applied Natural Science, Adama Science and Technology University, Adama P.O. 1888, Ethiopia

E-Mail: Abebe.aw45@gmail.com, enyewama@yahoo.com, detsegaye@gmail.com

Corresponding author: enyewama@yahoo.com

ABSTRACT

Fluoride contaminated drinking water is a major concern due to its negative health effects experienced by people in many parts of the world. This study focused on the synthesis of HAp and Fe doped HAp from diammonium hydrogen phosphate (DAP), calcium and iron precursors using urea as fuel for defluoridation of water and antibacterial activities. The synthesis of HAp and Fe doped HAp were characterized by using thermogravimetric analysis; scanning electron microscopy, X-ray diffraction, and Fourier transform Infrared spectroscopic techniques. An average crystallite size of HAp and Fe doped HAp were 32.54 nm and 27.91 nm, respectively, showing Fe doping results in a decrease in crystallite size. Batch adsorption studies were performed to investigate the adsorption capacity and removal efficiency of hydroxyapatite such as the effect of the initial pH of the solution, contact time, adsorbent dose and initial fluoride concentration. The adsorption data were fitted by Freundlich isotherm model and pseudo second order kinetic. In real water samples, the maximum removal efficiency of fluoride was observed to be 82.9 % with 4.2 mg/g maximum adsorption capacity under the optimum conditions which indicated that the prepared hydroxyapatite can be used as adsorbents for the removal of fluoride from contaminated real water with good efficiency. The antibacterial activities of the synthesized HAp and Fe doped HAp were tested against gram-negative bacterial strains E. coli and against gram-positive bacterial strains S. aureus using disc diffusion method. The maximum inhibition zone of gram-negative bacterial strains E. coli was 11 mm for both HAp and Fe doped HAp.

Keywords: Hydroxyapatite, Fe doped HAp, antibacterial activity, defluoridation, adsorbent

1. INTRODUCTION

Water is a very essential natural resource for life which may be contaminated by industrial wastes and natural sources.Groundwater is therefore the most attractive source for drinking water supply in the often scattered, rural communities in developing countries. Fluoride is one of the water quality parameters of concern, but the excess of which contaminates groundwater resources in many parts of the world, and renders it not drinkable for human ingestion, due to the related adverse health effects. Excessive intake of fluoride ions (>1.5 mg/L) can lead to various diseases such as fluorosis, cancer, osteoporosis, arthritis, brittle bones, thyroid disorder, and Alzheimer syndrome [1]. There is the negative health impact of excess fluoride in drinking water; however, the search for an appropriate technology for its removal from polluted-groundwater still remains very critical. Therefore, to solve this problem utilization of an appropriate removal technique and high fluoride removal capability material is crucial. Therefore, in order to prevent health hazards fluoride ion need to be removed from water using precipitation method, membrane method, ion exchange method, and adsorption method [2-4]. Among the above method, adsorption is considered more appropriate for defluoridation due to its simplicity, effectiveness, and economic viability. The parameters that influence the adsorption process are: pH value, initial concentration of adsorbate, contact time, temperature, the presence of other anions and the amount of adsorbent [5-7].

Recently, several researchers have investigated a range of calcium-based adsorbent biomaterials, of which synthetic hydroxyapatite (HAp) has been the promising candidate due to its identical chemical composition with bone, nontoxicity, and specifically high fluoride removal capability [6, 8, 9, 10]. Hydroxyapatite is chemically related to inorganic component of bone matrix as a complex structure with formula ($Ca_{10}(PO_4)_6(OH)_2$).This is referred to as stoichiometric hydroxyapatite and its atomic ratio Ca/P is 1.67.The Calcium-deficient (non-stoichiometric) of HAp, the Ca/P atom ratio is not 1.67. The chemical formula of stoichiometric hydroxyapatite (Ca_{10} $(PO_4)_6(OH)_2$), is 39 % by weight of Ca, 18.5 % P and 3.38 % of OH^- [11]. HAp was prepared by different methods such as hydrothermal method, precipitation methods, sol-gel method, combustion method, micro-emulsion method, ultrasonic synthesis method, microwave irradiation method and solid state method [12-19].

HAp can be synthesized from egg shell, fish scale, fish bone, bovine bone, calcium and phosphate source precursors and organic fuel [20-24]. In this study HAp can synthesis from iron, calcium and phosphate source precursors and urea. Fe is considered as a dopant in HAp, because it is, potentially less toxic than other transition metals [25]. HAp has an ability to inhibit the growth of bacterial activity. Drinkable water is often contaminated with microbes for instance; Escherichia coli (E. coli).Harmful strains of E. coli ingested in human body by various means can cause diarrhea, vomiting, severe anemia, kidney failure, urinary tract infections, and other infections [26]. Different concentrations of Fe doped HAp powder was mixed with amoxicillin powder in the ratio of 1: 0.5 showed a good inhibitory effect against gram negative bacteria E. coli reported by[27]. The aim of this study work was to synthesis high purity HAp and Fe doped HAp using urea as fuel and investigates their efficacy for defluoridation of water and antibacterial activity.

2. Materials and Methods

2.1. Raw materials

All analytical-grade chemicals and reagents used for the preparation of HAp were purchased from Addis Ababa chemical markets. Calcium nitrate tetrahydrate ($Ca(NO_3)_2 \cdot 4H_2O$, LOBA CHEMIE PVT.LTD, India, 98 %), di-ammonium hydrogen orthophosphate $(NH_4)_2HPO_4$, LOBA CHEMIE PVT.LTD, India, 97 %), urea $(CO(NH_2)_2$, LOBA CHEMIE PVT.LTD, India, 99 %), Iron nitrate nonahydrate ($Fe(NO_3)_3.9H_2O$, TECHNO PHARM CHEM. India, 98 %), nitric acid (HNO_3, LOBA CHEMIE PVT.LTD, India, 69 %), Sodium fluoride (NaF, BDH Chemicals Ltd. England, 97 %), tri-sodium citrate ($Na_2C_6H_2O_7$, BDH Chemicals, England, 99 %), Sodium Chloride (NaCl, LOBA CHEMIE PVT.LTD, India, 99.5 %), Etheyldiaminetetraacetic acid ($C_{10}H_{16}N_2O_8$, Brulux Laboratories (P), Ltd, India,99 %), glacial acetic acid (CH_3COOH, LOBA CHEMIE PVT.LTD, India, 99.7 %) and Sodium hydroxide (NaOH, SIGMA-ALORICH, Sweden, 98 %). Calcium nitrate tetrahydrate, di-ammonium hydrogen orthophosphate and Iron nitrate nonahydrate were used as precursor to synthesize the HAp and Fe doped HAp.

2.2. Experimental methods

2.2.1. Synthesis of Hydroxyapatite

50 mL of 0.6 M aqueous solutions of calcium nitrate tetrahydrate and 50 mL of 0.36 M aqueous solutions of DAP were added into 250 mL Pyrex beaker and continuously stirred with magnetic stirrer for 30 min till a white precipitate was formed by adjusting the molar ratio of Ca/P to 1.67. Concentrated nitric acid was added to dissolve the white precipitate and to adjust the pH value to 1.5 with stirring for 5 min. A predetermined amount of urea (as shown in Table 1) was added to the clear solution, and homogenized by stirring with a magnetic stirrer for 30 min at room temperature. The homogenized solution was heated on a hot plate at 100 ℃ for 2:30 hr to remove the excess solvent. The foam gel agglomerate product was formed and then the gel agglomerate was dried in oven at 200 ℃ for 1 hr. Then the dried gel agglomerate was grounded with mortar and pestle into fine powder and calcinated at 700 ℃. The synthesized HAp powder was stored in a dry place and taken for further characterization.

Table 1: Batch compositions for HAp

Sample code	Amount			
	$Ca(NO_3)_2.4H_2O$ Mole	$(NH_4)_2HPO_4$ Mole	Urea Mole	Combustible amount (urea to calcium precursor mass ratio)
HAp_1	0.03	0.018	0.118	1
HAp_2	0.03	0.018	0.118	2
HAp_4	0.03	0.018	0.236	4

Where HAp_1, HAp_2 and HAp_4 represent synthesized hydroxyapatite urea to calcium precursor mass ratio 1:1, 2:1 and 4:1, respectively. Table 1 show that the Ca/P molar ratio was maintained at the value of 1.67 for all optimized hydroxyapatite.

2.2.2. Synthesis of Iron- doped Hydroxyapatite

Fe doped HAp was synthesized by using different mole of Fe and keeping other precursors mole constant. $(Ca_{10-x}Fe_x\ (PO_4)_6(OH)_2$, with x = 0.01, x = 0.03, x = 0.05, x = 0.07 and x = 0.1. $Ca(NO_3)_2.4H_2O$ and $Fe(NO_3)_3.9H_2O$ were dissolved together in deionized water in beaker to obtain 50 mL [Fe + Ca] containing solution. Then, $(NH_4)_2HPO_4$ was dissolved in deionized water in other beaker to obtain 50 mL P-containing solution. 50 mL of 0.6 M aqueous solutions of calcium nitrate tetrahydrate and iron nitrate nonahydrate [Ca + Fe] and 50 mL of 0.36 M aqueous solutions of DAP were added into 250 ml Pyrex beaker and continuously stirred with magnetic stirrer for 30 min till a precipitate was formed. Concentrated nitric acid was added, with stirring for 5 min, to dissolve a precipitate and to adjust the pH value at 1.5. Predetermined amount of urea (as shown in Table 2) was added as fuel to the clear solution which was homogenized by stirring with a magnetic stirrer for 30 min at room temperature. The Urea mass was selected from the three ratio of the synthesized HAp which has the highest fluoride removal efficiency. The homogenized solution was heated on a hot plate at 100 ℃ for 2:30 hr to remove the excess solvent. The agglomerate gel was formed and then the gel agglomerate was dried in oven at 200 ℃ for 1 hr. Then, the dried gel agglomerate was grounded with mortar and pestle into fine powder and calcinated at 700 ℃. The synthesized Fe doped HAp powder was stored in a dry place and taken for characterization.

Table 2: Batch composition for Fe doped HAp

Sample code	Amount			
	$Ca(NO_3)_2.4H_2O$ Mole	$Fe(NO_3)_3.9H_2O$ Mole	$(NH_4)_2HPO_4$ Mole	Urea Mole
$Fe_{0.01}$ HAp	0.02997	0.00003	0.018	0.472
$Fe_{0.03}$ HAp	0.02991	0.00009	0.018	0.472
$Fe_{0.05}$ HAp	0.02985	0.00015	0.018	0.472
$Fe_{0.07}$ HAp	0.02979	0.00021	0.018	0.0472
$Fe_{0.1}$ HAp	0.0297	0.0003	0.018	0.0472

Before Fe doped HAp was synthesized the removal efficiency of HAp was evaluated. Then, the synthesized HAp which has high fluoride removal efficiency was selected. Table 2 show that the moles of DAP and urea were constant but, the moles of calcium and iron precursors were changed. That is as mole of iron precursor increase, mole of calcium precursor decrease. The (Fe + Ca)/P molar ratio was maintained at the value of 1.67 for all optimized Fe doped hydroxyapatite.

2.3. Methods of data analysis

The synthesized biomaterials were analysis by difference techniques.TGA/DTA analysis was used (Model DTG-60H, Shimadzu Co., Japan) for the determination of the calcination temperature. 10 mg of HAp and 12.083 mg Fe doped HAp were taken and placed in the alumina crucible for TGA/DTA analyzed at the heating rate of 20 ℃/ min with a constant supply of non-stop glide of nitrogen. FTIR (Model FT/IR-6600 type A, JASCO, Japan) was used in a transmission mode of the mid-infrared range with wave numbers from 400 to 4000 cm^{-1} using the potassium bromide (KBr) pellet technique. KBr pellets were made by mixing 2 mg of HAp powder with 12 mm diameter die 200 mg of KBr using mortar and pestle, compressed to form the pellet and then placed on a specimen holder. Spectra were measured between in the range of 4000 cm^{-1} to 400 cm^{-1} at a resolution of 4 cm^{-1}, with number of scans 8 and scanning speed 2 mm/sec.The synthesized HAp and Fe doped HAp morphology were analyzed using SEM (model JEOL JCM-6000plus, Japan). Electron beam energy of HAp and Fe doped HAp were carried out

at accelerate voltage at 15 Kv and magnification of 600. XRD analysis was used to identify crystalline size, crystalline structure, miller indices and space group present in a synthesized HAp and Fe doped HAp were characterized using an X-ray diffractometer (XRD-700, Shimadzu Co., Japan). A Cu target for generating a Cu Kα radiation (λ = 1.54056 Å) was used as the incident X-ray beam at an accelerating voltage of 40 kV and a current of 30 mA. The powder samples were mounted on a flat XRD plate and scanned in the range 10º to 85º at room temperature in the continuous scan speed 3 (deg/min). The step size and the time per step were 0.02 (deg) and 0.40 sec respectively.

2.4. Collection of Water Sample for the defluoridation Test.

Three samples of ground water were collected from Tuch Danbali located at East Shewa Meki district. The samples were taken in 500 mL in high land. Before the samples were taken in high land, a high land was washed three times by raw water. Then, the pH and fluoride ion concentration of ground water was measured. From the three samples the high pH and high fluoride concentration 8.2 and 6.9 mg/L was selected, respectively. Then, 20 mL of ground water, 15 mL of deionized water and 3 mL of TISAB were added into one beaker. Then, the concentration of fluoride in ground water was measured by using fluoride ion selective electrode.

2.5. Determination of fluoride

2.5.1. Preparation of Stock Solution

2.21 g of sodium fluoride was weighed and transferred into 1000 mL volumetric flask. Then, it was dissolved by deionized water and diluted to 1 L. The prepared solution containing 2210 mg/L stock solution of sodium fluoride or 1000 mg/L stock solution of fluoride ion. From the stock solution 100 mg/L intermediate solution was prepared. From this intermediate solution, four samples of fluoride solutions of 10, 15, 20 and 25 mg/L were prepared by serial dilution for the defluoridation test.

2.5.2. Preparation of Total Ionic Strength Adjustment Buffer (TISAB)

TISAB is essential in fluoride ion selective electrode measurements because it masks minor changes made in the ionic strength of the solution, maintain pH constant and hence increases the accuracy of the reading. 7 g of tri-sodium citrate ($Na_2C_6H_2O_7$), 58 g sodium chloride (NaCl), and 2 g EDTA were dissolved into 500 mL of distilled water. Then, 57 mL of glacial acetic acid

was added into the solution. Finally, 5 M of sodium hydroxide was added till the pH of the solution was reached at 5.3 and then the solution was transferred to a 1000 mL volumetric flask, and filled up to the mark using distilled water.

2.5.3. Calibration of the Electrode

Before calibration of the electrode, the reference electrode hole was filled with KCl solution and the electrode was stored in TISAB solution. Then, the electrode was rinsed with distilled water to minimize contamination. 2 ppm, 4 ppm, 6 ppm, 8 ppm and 10 ppm of fluoride solution were prepared. To 30 mL of each five fluoride solutions 3 mL of TISAB was added in order to maintain pH constant and increases the accuracy of the reading. Then, the potential response of fluoride ion was measured starting from low concentration to high concentration using fluoride ion selective electrode. Finally, to determine the slope of the graph, the potential response (E in mV) versus the negative logarithm of concentration (- log C in mg/L) was plotted.

2.6. The pH at point of zero charges (PZC)

To identify the working pH value for adsorption studies the point of zero charge was determined before optimization of pH. 50 mL of 0.1 M NaCl solutions were taken in eight conical flasks with pH range 2 – 9 by 1 pH increment and the pH was adjusted by using 0.1 M HCl and 0.1 M NaOH. Then, 0.5 g of Fe doped HAp powder was added to each solution and vibrated by using mechanical shaker at a speed of 150 rpm for 10 hr. Then, the adsorbent was separated from the solutions by using filter paper and funnel. After equilibration the final pH of each sample was measured by using pH meter. Then, the change in pH (ΔpH) was calculated (ΔpH = final pH – initial pH). Finally, to determine the pH at pzc, the graph of change in pH vs. final pH was plotted.

2.7. Optimization of Different Parameters

In this study, the effect of major parameters like pH, adsorbent dose, contact time and initial fluoride concentration were optimized to investigate the maximum defluoridation efficiency of the synthesized iron doped hydroxyapatite.

2.7.1. Effect of pH

To study the effect of pH on defluoridation, 50 mL of 10 mg/L of fluoride solution was taken and pH values was adjusted to 3, 5, 7 and 9 by using 0.1 N HCl and 0.1 N NaOH and 0.5 g of

adsorbent dose was used in acidic, neutral, and basic media. Then, the solution was shaken by using mechanical shaker at a speed of 150 rpm for 5 hr. After a given time was completed the solution was filtered. 3 mL of TISAB was added to each solution in order to maintain pH constant and stirred with magnetic stirrer. Then, the F^- ion concentration of filtrate solution was determined by using fluoride ion selective electrode.

2.7.2. Effect of Adsorbent Dosage

To study the effect of the synthesized Fe doped HAp dose on defluoridation, 50 mL of 10 mg/L of fluoride solution was adjusted to a pH of 3. Then various dosages of Fe doped HAp (0.1 g, 0.3 g, 0.5 g, 0.7 g, and 0.9 g) were added into the solution. Then the solution was shaken by mechanical shaker at a speed of 150 rpm for 3 hr. After 3 hr was completed the solution was filtered. 3 mL of TISAB was added to each solution in order to maintain pH constant and stirred with magnetic stirrer. Then, the F^- ion concentration of filtrate solution was determined by using ion selective electrode.

2.7.3. Effect of Contact Time

To study the effect of contact time on defluoridation, 50 mL of 10 mg/L of fluoride solution was adjusted to a pH of 3. Then 0.7 g of Fe doped HAp with high removal efficiency of fluoride was added into each solution and shaken by mechanical shaker at a speed of 150 rpm for different contact time (1 hr, 3 hr, 5 hr and 7 hr). After these periods of intervals, the solution was filtered. 3 mL of TISAB was added to each solution in order to maintain pH constant and stirred with magnetic stirrer. Then, the F^- ion concentration of filtrate solution was determined by using ion selective electrode.

2.7.4. Effect of initial concentration of fluoride ion

To study the effect of initial concentration of fluoride ions on defluoridation, 50 mL of fluoride solutions with different concentration (10, 15, 20 and 25 mg/L) were taken and then, the pH was adjusted at 3. Then 0.7 g of Fe doped HAp with high removal efficiency of fluoride was added into each solution. Then, the solution was shaken by mechanical shaker at a speed of 150 rpm for 3 hr. After 3 hr was completed the solution was filtered. 3 mL of TISAB was added to each solution in order to maintain pH constant and stirred with magnetic stirrer. Then, the F^- ion concentration of filtrate solution was determined by using ion selective electrode.

2.7.5. Defluoridation Test

The concentration of fluoride ion in ground water was measured by using optimized parameters. 50 mL of 6.9 mg/L of ground water was taken into a beaker. 0.7 g Fe doped HAp dosage was added into the solution in the beaker. Then, the solution was shaken by mechanical shaker at a speed of 150 rpm for 3 hr at pH 3. After 3 hr was completed the solution was filtered. Then, 3 mL of TISAB was added to the solution in order to maintain pH constant and stirred with magnetic stirrer. Finally, the F^- ion concentration of filtrate solution was determined by using ion selective electrode.The fluorideremoval efficiency and adsorption capacity were calculated using the following Equations 1 and 2:

$$\text{Removal efficiency} = \left(\frac{C_o - C_f}{C_o}\right) \times 100 \quad \ldots\ldots (1)$$

$$\text{Adsorption capacity} = \left(\frac{C_o - C_o}{m}\right) V \quad \ldots\ldots (2)$$

Where Co is initialfluoride concentration, Cf is final fluoride concentrations, m is the mass of the adsorbent and V is the volume of the solution.

2.8. Adsorption Isotherm Models.

Adsorption isotherm is the relationship between the adsorbate and the adsorbate adsorbed on the surface of the adsorbent at equilibrium at constant temperature. Langmuir and Freundlich isotherms provide information on the nature and physic-chemical interactions involved in the adsorption [28]. These two-parameter models are simple and give a good description of experimental behavior in a large range of operating conditions.

2.8.1. Langmuir Adsorption Isotherm

The Langmuir adsorption isotherm is used to describe the equilibrium between adsorbate and adsorbent system, where the adsorbate adsorption is limited to monolayer at or before a relative pressure of unity is reached.Langmuir adsorption isotherm model was expressed by the following linear equation (Equation 3):

$$\frac{1}{qe} = \frac{1}{b\, Q_{max}\, Ce} + \frac{1}{Q_{max}} \quad \ldots\ldots (3)$$

Where Ce (mg/L) is the equilibrium concentration of the adsorbate, Q_{max} (mg/g) and b (L/mg) isLangmuir constants related to sorption capacity and rate of sorption, respectively.

2.8.2. Freundlich Adsorption isotherm

Freundlich adsorption isotherm is considered to be a multilayer process in which the amount of adsorbed solute per unit adsorbent mass increases gradually.Langmuir adsorption isotherm model was expressed by the following linear equation (Equation 4):

$$\text{Logqe} = \frac{1}{n}\text{Log}Ce + \text{Log}K \quad \text{..... (4)}$$

Where qe (mg/g) is the amount of adsorbate per unit mass of adsorbent,K and n are the indicators of adsorption capacity and adsorption intensity, respectively.

2.9. Adsorption Kinetics model

The adsorption kinetic models describe the rate of uptake of the adsorbate molecule; in this case, fluoride ion onto adsorbent, the rate depends on the physicochemical characteristics of the adsorbate and adsorbent, pH, temperature, and concentration.Pseudo first order and pseudo second order models are very common to describe adsorption kinetics model.Pseudo first order and pseudo second order models were expressed by the following linear equation (Equations 5 and 6):

The linear equation of Pseudo first order model: $\text{Log (qe} - \text{qt)} = \text{Log qe} - \frac{K_1}{2.303}t$ ..... (5)

The linear equation of Pseudo second order model: $\frac{t}{q_t} = + \frac{t}{q_e} + \frac{1}{K_2 q_e^2}$ ..... (6)

Where pseudo first order constant (K_1), pseudo second order constant (K_2), equilibrium adsorption capacity (qe) and equilibrium adsorption capacity at a given t (qt). K_1, K_2 and qe can be determined from the slope and intercept of plotted graph log (qe- qt) versus t, and t/qt versus t, respectively. Logqe is the intercept and $-k_1$ is the slope for pseudo first order kinetics. $\frac{1}{K_2 q_e^2}$ is the intercept and $\frac{1}{qe}$ is the slope forpseudo second order kinetics.

2.10. Regeneration and Desorption of Adsorbent

To study the regeneration and desorption of adsorbent on defluoridation, 50 mL of 10 mg/L of fluoride solution was taken in beaker and 0.7 g of Fe doped HAp powder was added. The pH of the solution was adjusted at 3 and was shaken by using mechanical shaker at a speed of 150 rpm for 3 hr. After adsorption the adsorbent was separated by filtration. The filtrate concentration of fluoride was measured and removal efficiency of fluoride was calculated for the first cycle. Then, the residual of adsorbent was dispersed in 50 mL of 1 N NaOH to be desorbed and shaken for 1 hr. After 1 hr the solution was decanted and the residual adsorbent was dried in oven for 30 min at 150 ℃. The dried residual adsorbent mass was measured and regenerated for fluoride adsorption again. Five cycles of desorption and regeneration was performed using the same procedure.

2.11. Antibacterial Activity

Antibacterial activities were carried out against two bacterial strains; gram-negative E. coli and gram positive S. aureus bacteria by disc diffusion method. 30 mg of each prepared samples were dissolved in 1 mL dimethyl sulfoxide (DMSO). Bacterial cultures were maintained on nutrient Muller-Hinton agar at 37 ˚C, the antibiotic Contrimoxazole was used as the positive control and DMSO solvent was used as the negative control. From 30 mg/mL concentration of sample, 15 mg/mL, 7.5 mg/mL and 3.75 mg/mL were prepared by diluting serially. Then, 6 mm diameter disc was saturated with 20 µL from each concentration and 20 µL of 0.5 mg/ mL of Contrimoxazole (positive control) and placed on a plate and covered with lids and incubated at 37 °C for 24 h. Antibacterial activity was evaluated by measuring the diameter of the inhibition zone observed around the discs. The inhibition zone reveals the bacteria sensibility to toxic agents so that the disinfectant-sensitive strains show large inhibition diameter and the resistant strains show a smaller or zero inhibition diameter. This diameter can be compared to the critical diameters of antibiotics Contrimoxazole and digital images were captured [29].

3. RESULTS AND DISCUSSION

3.1. Thermo gravimetric Analysis and Differential thermal analysis

The thermal analysis of synthesized HAp was investigated by TGA/ DTA analytical technique. TGA curve shows weight loss of the sample, whereas the DTA curve indicates the energy gain or loss during the process. Synthesized biomaterial TGA analysis was measured from 31.26 °C to 800 °C at the heating rate 20 °C /min with a nonstop glide of nitrogen. The TGA curves of the synthesized HAp presents a total weight loss of about 4.41 mg (44.1 %) with occurring in three inflection points. The three inflection points were the evaporation of absorbed water, dehydration of hydroxides and removal of ammonia, and decomposition of volatile organic impurities. As Figure 1 shows that from 31.26 °C to 200.63 °C, 0.539 mg (5.39 %) weight loss was observed. From 200.63 °C to 445.64 °C, 3.84 mg (38.4 %) weight loss was observed. From 445.64 °C to 700 °C, 0.031 mg (0.31 %) a slight weight loss was observed. Figure 1 DTA curve shows that all peaks are endothermic, there is no exothermic peak was observed.

The TGA/DTA curves of the synthesized Fe-HAp analysis in the range of 23.79 °C to 1001.71 °C at the heating rate 20 °C / min with a nonstop glide of nitrogen. The TGA curves of the synthesized biomaterial presents a total weight loss of about 10.71 mg (88.63 %) with occurring in three inflection points. Figure 2 shows that 0.59 mg (4.88 %) weight loss was observed from 23.79 °C to170.52 °C. 9.16 mg (75.81 %) weight loss was observed from 170.52 °C to 364.33 °C. Also 0.96 mg (7.94 %) weight loss was observed from 364.33 °C to 700 °C. Figure 2 DTA curve shows that the reaction at 558.06 °C was released energy, this is due to exothermic peak was observed. From TGA analysis there is no weight loss after 700 °C. Therefore, 700 °C is the calcination temperature of synthesized HAp and Fe doped HAp.

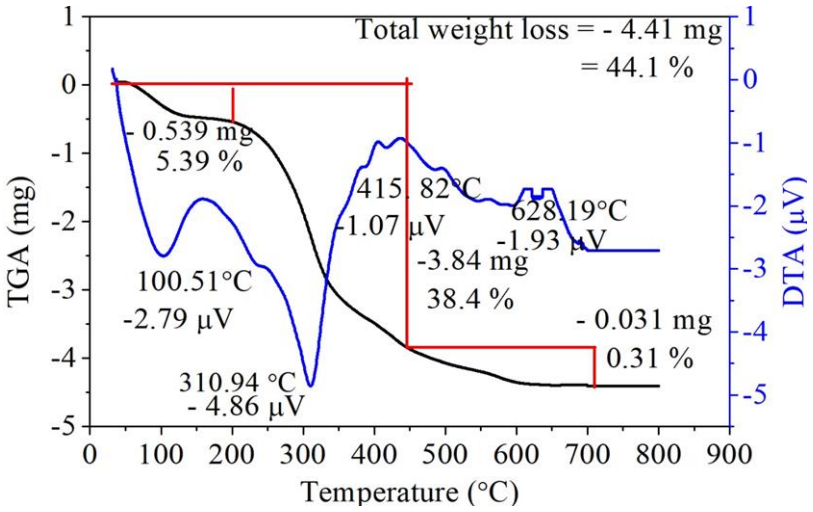

Figure 1: The result of TGA and DTA analysis of HAp

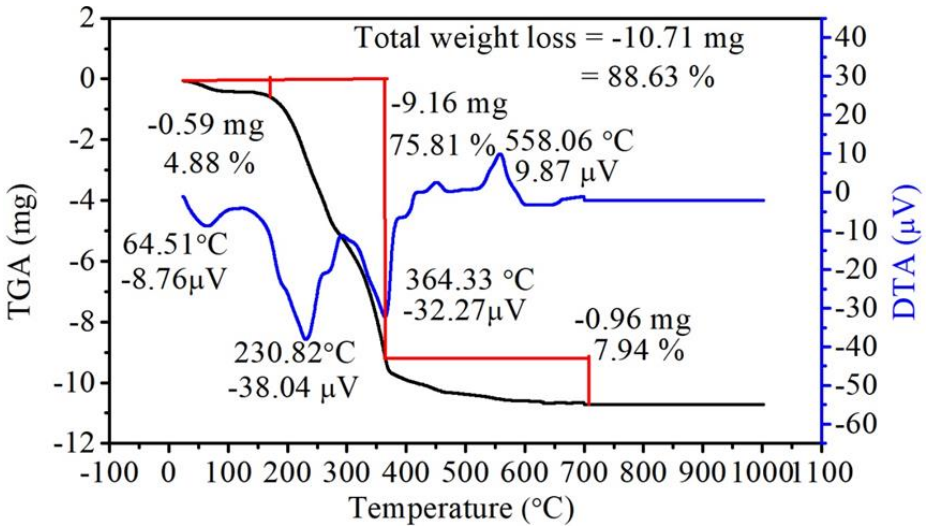

Figure 2: The result of TGA and DTA analysis of Fe doped HAp

3.2. X–ray diffraction analysis result

Crystalline structure, miller indices and space group of synthesized HAp and Fe doped HAp were characterized using XRD patterns. Figure 3 shows the XRD spectra of HAp and Fe doped HAp synthesized using 4:1 urea mass to calcium precursor mass and mole of iron at x=0.05. For HAp diffraction peaks were observed at 2θ values, 26.12º, 31.14º, 32.16º and 34.46º which corresponds to (002), (211), (112), and (202) plane which confirm the formation of HAp, respectively. All the XRD peaks of synthesized HAp showed hexagonal phase and the observed peaks were fitted with the standard (JCPDS card No. 00-009-0432, space group P63/m. Also the diffraction peaks of Fe doped HAp observed at 2θ positions 26.16º (002), 31.7º (211), 32.2º

(112), 34.72º (202) shows the formation similar crystallized hexagonal hydroxyapatite structure, similar result was reported by [30].

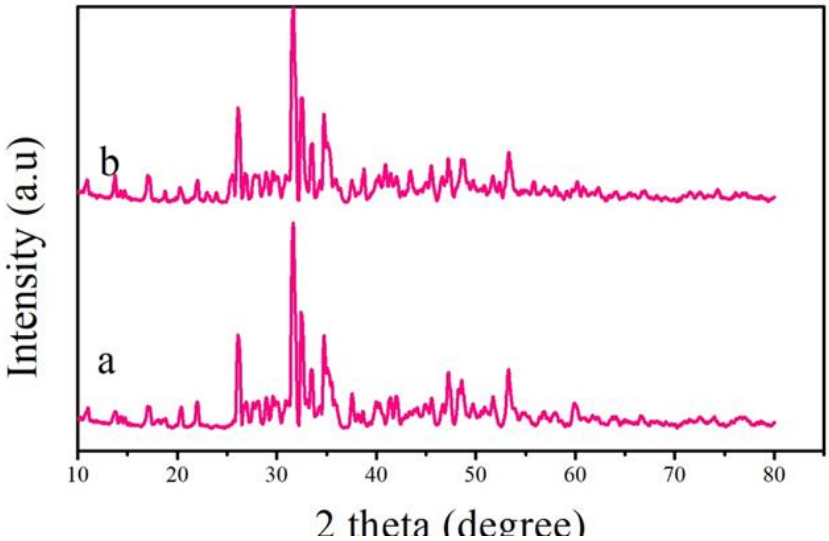

Figure 3: Result of X-ray Diffraction a) hydroxyapatite and b) iron doped hydroxyapatite

The crystallite size and average crystallite size of the synthesized HAp and Fe doped HAp powders were determined from the peak broadening.Scherrer's formula was used to determine the crystal size from the XRD pattern using the following Equation7:

$$D = \frac{K\lambda}{\beta Cos\theta} \quad \text{..... (7)}$$

Where, D is the crystallite size (nm), k is the Scherer constant (0.94 for spherical hexagonal structure), λ is the wavelength of the X-ray radiation (0.15406 nm), and β is the experimental full width at half maximum intensity of the diffraction peak under the consideration peak; θ is the diffraction angle (degree).

The crystallite size of HAp was 32.54 nm and the crystallite size of Fe doped HAp was 27.91 nm, which is a similar result as reported by [31]. This indicated that the addition of Fe into HAp decreases the crystallite size. This is due to the ionic radius of Fe^{3+} (0.064 nm) is smaller than that of Ca^{2+} (0.099 nm). For the addition of Fe into HAp, it can be assumed that every two Fe^{3+} ions substitute with three Ca^{2+} ions to arrange for the ionic balance [31].

The lattice parameters was described the properties of the synthesized material. The lattice parameters of HAp and Fe doped HAp were calculated by using major peaks. Lattice parameters of hexagonal structure of HAp and Fe doped HAp can be calculated by Equations 8:

$$\frac{1}{d^2_{hkl}} = \frac{4}{3a^2}(h^2 + hk + k^2) + \frac{l^2}{c^2} \quad \text{..... (8)}$$

Where,a and c arelattice parameters (Å).The lattice parameters (a and c) were calculated from the two miller indices (300) and (002) planes corresponding to peak position 33.1º and 26.12º, respectively. For the first miller indices the value of h =3, k and l = 0. For the second miller indices the value of l = 2, h and k = 0. For HAp lattice constant: a = 9.40 Å, c = 6.818 Å. For Fe doped HAp lattice constant: a = 9.34 Å, c = 6.806 Å. From the calculation the lattice constant a and c decreases from 9.40 Å to 9.34 Å, 6.818 Å to 6.806 Å, respectively. The lattice parameters slightly decreased as the Fe^{3+} was introduced due to the difference in the ionic radii of iron (0.64 Å) compared to Ca^{2+} (0.99 Å) [32].

3.3. Fourier-Transform Infrared Spectroscopy

The functional group and additional impurities were characterized by Fourier-Transform Infrared Spectroscopy. The functional groups of HAp and Fe doped HAp compositions $Ca_{10-x}Fe_x(PO_4)_6(OH)_2$ at x= 0.05 were characterized using FT-IR spectra in the range 4000 - 400 cm^{-1}. Figure 5 shows that the formation of hydroxyapatites clearly seen in FTIR spectra of all FTIR spectra. The vibrational frequencies were observed due to the presence of PO_4^{3-}, OH^- functional groups and lattice vibrations for hydroxyapatite. From (Figure 4) there are four main absorption regions; the symmetric P-O stretching bands (900 - 1000 cm^{-1}), symmetric O-P-O bending mode (400 - 500 cm^{-1}), asymmetric P–O stretching bands (1000 – 1200 cm^{-1}) and asymmetric O-P-O bending mode (500 – 700 cm^{-1}) [33]. The functional group PO_4^{3-}, absorption peak of asymmetric P–O stretching at 1026 cm^{-1} and 1135cm^{-1}, absorption peak of P–O bending at 558 cm^{-1}, absorption peak of symmetric P–O stretching vibrations at 931 cm^{-1} and absorption peak bending vibration of O-P-O at 495 cm^{-1} and 450 cm^{-1}were observed confirming the formation of the hydroxyapatite. A broad peak observed at 3437 cm^{-1} depicts the lattice vibration of OH^- stretching. The absorption peak of hydroxyl groups (OH^-) bending mode appeared at 1639 cm^{-1}, due to adsorbed water on the HAp surface. An absorption band observed in the synthesized samples at 1639 cm^{-1} the presence of physically adsorbed water [34].

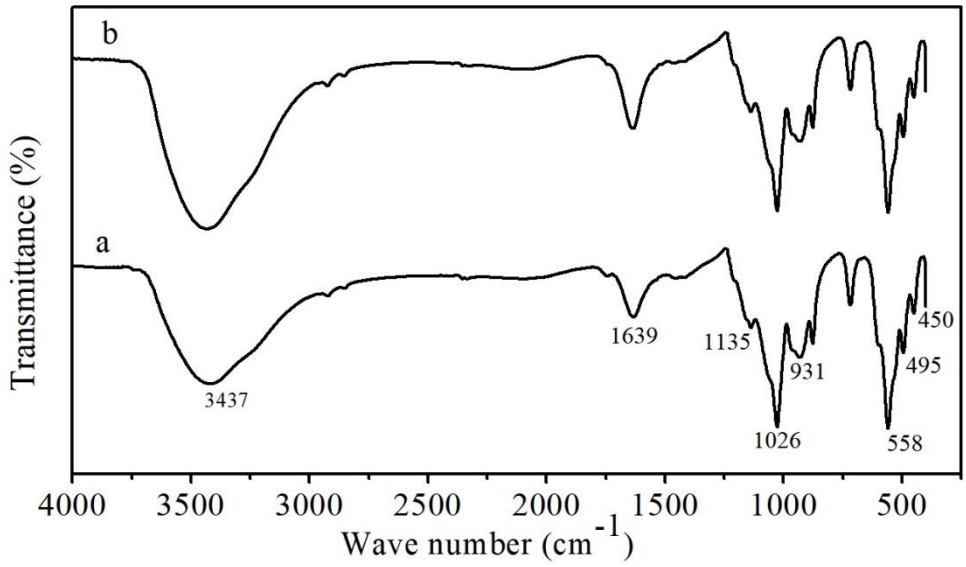

Figure 4: Result of FT-IR a) hydroxyapatite and b) iron doped hydroxyapatite

3.4. Scanning electron microscopy (SEM)

The surface morphology of synthesized pure HAp and Fe-HAp crystals were studied using SEM image. As Figure 5 (a - b) shows that the SEM images of both pure HAp and Fe doped HAp (at x = 0.05) synthesized with urea fuel were agglomerated and without clear grain morphologies.

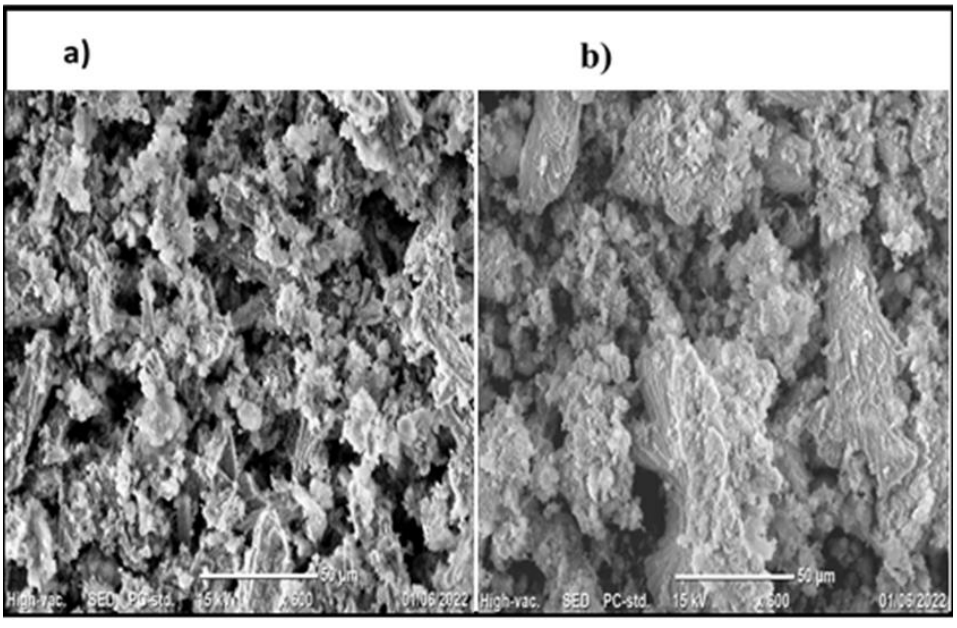

Figure 5: The SEM image a) HAp b) Iron doped HAp

3.5. The pH at point of zero charge

The pH of pzc determination of Fe doped HAp was carried out at pH 2 - 9 by one pH unit increment. Figure 6 shows the point of zero charge is 7.5 in agreement with [5, 10]. Below the point of zero charge the adsorbent has positive charge while above the point of zero charge it has negative charge. The higher fluoride adsorption was occurred under pH 7.5 due to highly electrostatic attraction between the positively charged adsorbent surface and highly electro negative fluoride ions. The low fluoride adsorption was occurred above pH 7.5 due to weak electrostatic attraction between the negatively charged adsorbent surface and highly electro negative fluoride ions.

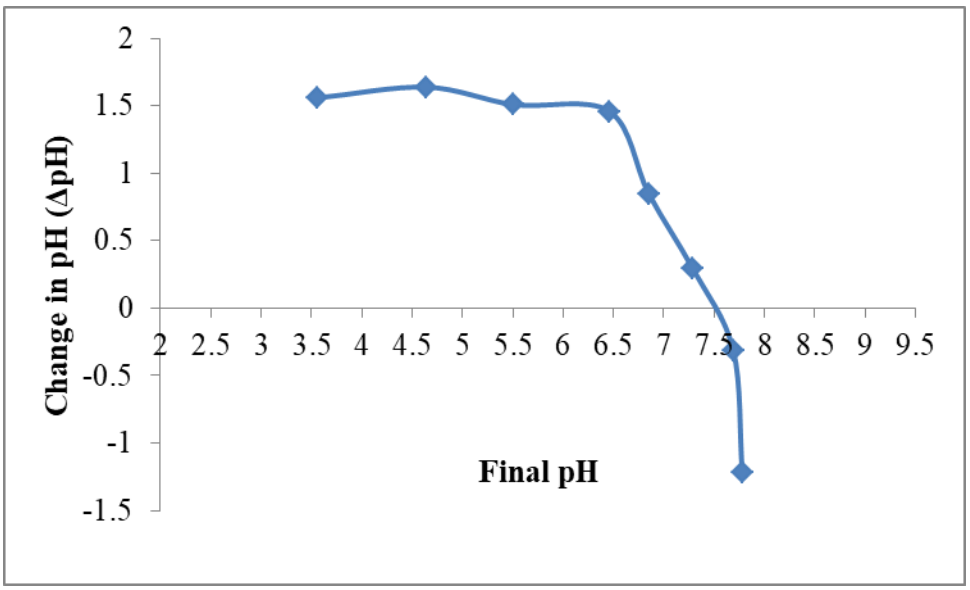

Figure 6: Plot of Δ pH vs. final pH of the adsorbent to determine the point of zero charge.

3.7. Calibration of Fluoride Ion Selective Electrode

The fluoride ion selective electrode was calibrated by using different fluoride ion concentration of standard solution. The graph of calibration curve was plotted by potential response (E in mV) vs. negative logarithm of fluoride concentration (- LogCe in mg/L) as shown in (Figure 7). The slope of the graph and R^2 were determined from the curve to check the accuracy of the measurement. The slope of fluoride ion should be in the range 54 - 60 mV L mg-1. From (Figure 7) the slope was observed between the standard intervals with good R^2 values. From the plotted graph, the slope was found to be 57.93 mV L/mg and R^2 value 0.9954, which is nearest to one.

Therefore, the fluoride concentrations were calculated using the regression equation E = 57.93 (-Log Ce) - 64.876 (Figure 7).

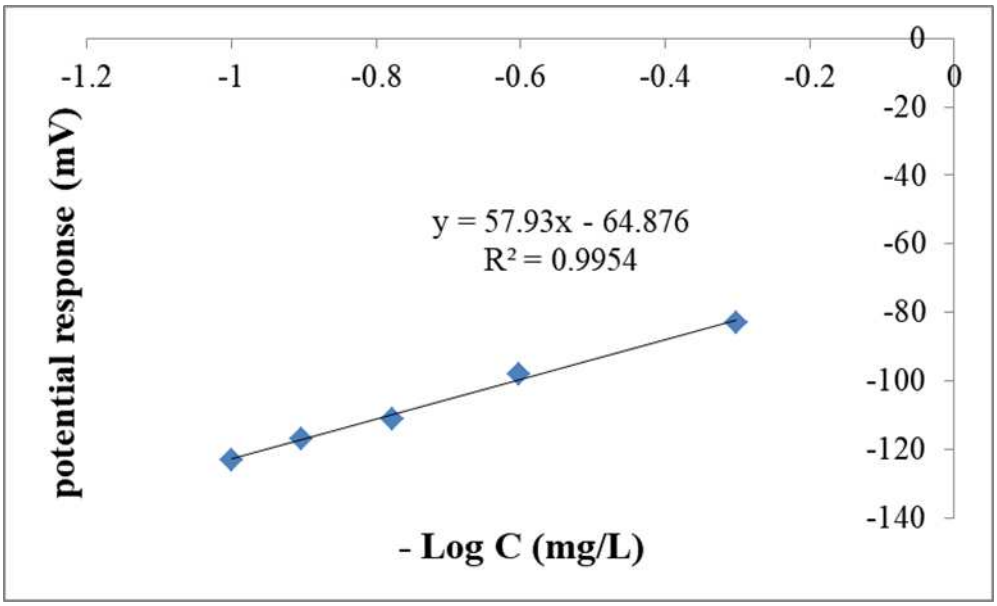

Figure 7: Electrode calibration E versus – LogCe of fluoride concentration

3.8. Optimization of Different Parameters for Adsorption Study

The fluoride removal efficiency of HAp for HAp_1, HAp_2 and HAp_4 were recorded as 90.7 %, 92.1 % and 95.1 %, respectively. The effectiveness of HAp on the removal of fluoride ion was carried out by using adsorbent dosage 0.5 g, pH 3, initial concentration of fluoride ion solution 10 mg/L, volume of fluoride solution 40 mL, and shaking speed 150 rpm for 5 hr. After the removal efficiency of HAp was evaluated, and then Iron was doped to HAp which has high removal efficiency. To investigate the removal Potential of Fe doped HAp all iron doped HAp adsorbent removal efficiency were evaluated. The removal efficiency of $Fe_{0.01}$HAp, $Fe_{0.03}$HAp and $Fe_{0.05}$HAp, $Fe_{0.07}$HAp and $Fe_{0.1}$HAp were recorded to be 91.1 %, 91.8 %, 96.1 %, 93.2 % and 90.3 %, respectively. From this result as urea to calcium precursor mass ratio increases the removal efficiency of fluoride ion increases. Also as concentration of iron doped HAp increases the removal efficiency of fluoride ion increases. But after 0.05 mole of Fe doped HAp the removal efficiency of fluoride ion decreases. The lattice parameters, crystallinity, crystallite size, particle size and morphology values are affected by increasing Fe content. However, the

applications of Fe doped HAp are strongly influenced by crystallinity, particle size, porosity, morphology and other external conditions [33].

a). 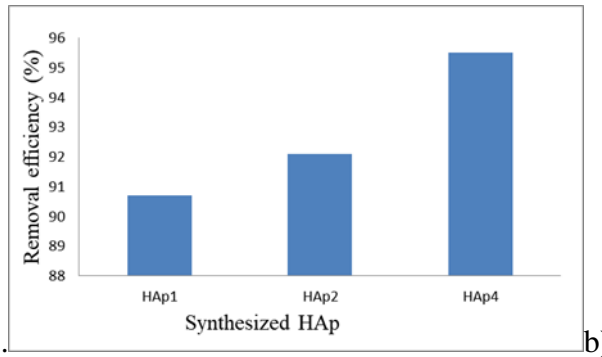

b) 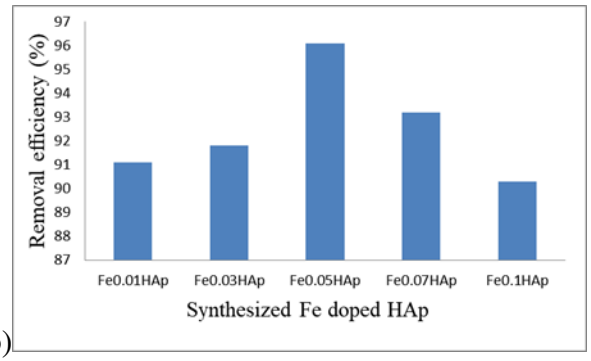

Figure 8: Removal efficiency of a) HAp and b) Fe doped HAp by different ratio

3.8.1. Effect of pH on removal of fluoride ion by Fe doped HAp

During the adsorption process, determination of pH of the solution was very important. The pH of the solution was tested in acidic, neutral, and basic media. The effect of pH on the removal of fluoride ion was carried out by keeping all parameters constant like adsorbent dosage 0.5 g of Fe doped HAp, initial concentration of fluoride ion solution 10 mg/L, volume of fluoride solution 50 mL, and shaking speed 150 rpm for 5 hr. The effect of pH was determined by using the pH interval from 3 to 9 with 2 increments. Figure 9 shows that the maximum removal efficiency of fluoride ion was achieved at pH 3 which is 95.6 %. From the result of pH optimization, it was observed that at high pH values the removal of fluoride ion was low and high at low pH values. In acidic medium, where the concentration of H^+ ion is high and therefore HAp surface gets positive charge which in turn attracts more fluoride ions and hence there is a significant increase in fluoride removal capacity at lower pH. The high uptake at low pH was attributed to the high concentration of hydrogen ions at low pH which increases the positive charge on the surface of the adsorbent leading to greater removal of fluoride ion [35].

At pH above the pzc, adsorption of fluoride ion was low because the HAp surface was negatively charged, due to deprotonation of HAp hydroxyl groups [5]. There was repulsive force between the negatively charged of fluoride ion and the negatively charged adsorbent surface. Due to this repulsive force between the two negatively charged ions the removal of fluoride ion was decrease.

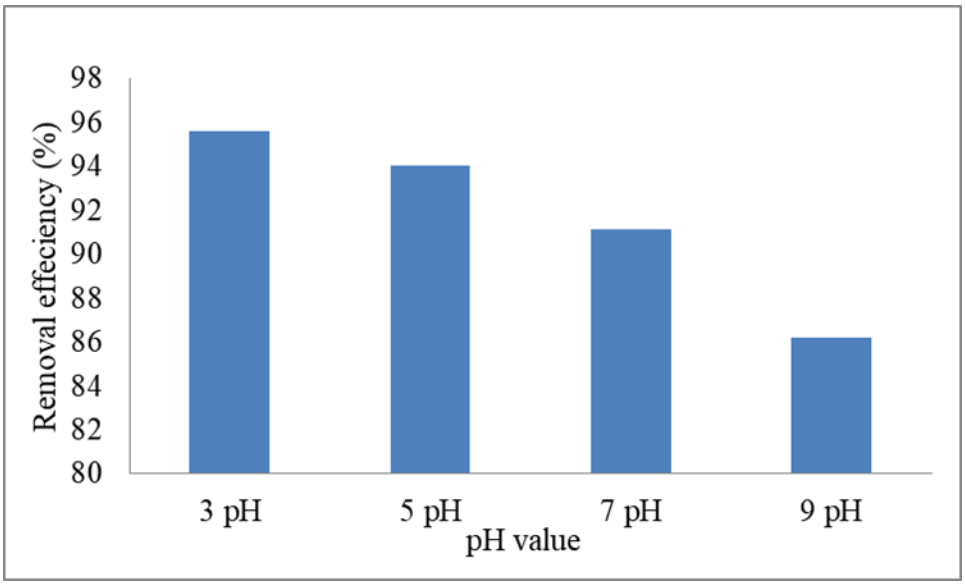

Figure 9: Effect of solution pH on removal efficiency of fluoride ion

3.8.2. Determination of adsorbent dosage

Determination of adsorbent dosage of the synthesized material was very important during the adsorption process. The effect of adsorbent dosage was optimized by taking different masses. The effect of adsorbent dosage was carried out by keeping all parameters constant like initial concentration of fluoride ion solution 10 mg/L, volume of fluoride solution 50 mL, pH 3, at shaking speed 150 rpm for 5 hr. The effect of adsorbent dosage was determined by using the adsorbent dosage interval from 0.1 g to 0.9 g with 0.2 increments. As (Figure 10) shows that the maximum removal efficiency of fluoride ion was achieved at adsorbent dosage of 0.7 g which is 96.1 %. As (Figure 10) result indicates that the removal efficiency of fluoride ion increases as Fe doped HAp dosage increases up to 0.7 g at optimum dose. This is because at high doses there is high availability of active sites. The number of binding sites resulting from increased adsorbent dosage and availability of more effective sites for interaction contributed to the observed result [35]. But the removal efficiency of fluoride was decreased at 0.9 g dosage due to the overlap or blocking of functional surface sites of adsorbent. Another reason is due to the depletion of fluoride in the solution with an increasing dose of the adsorbent.

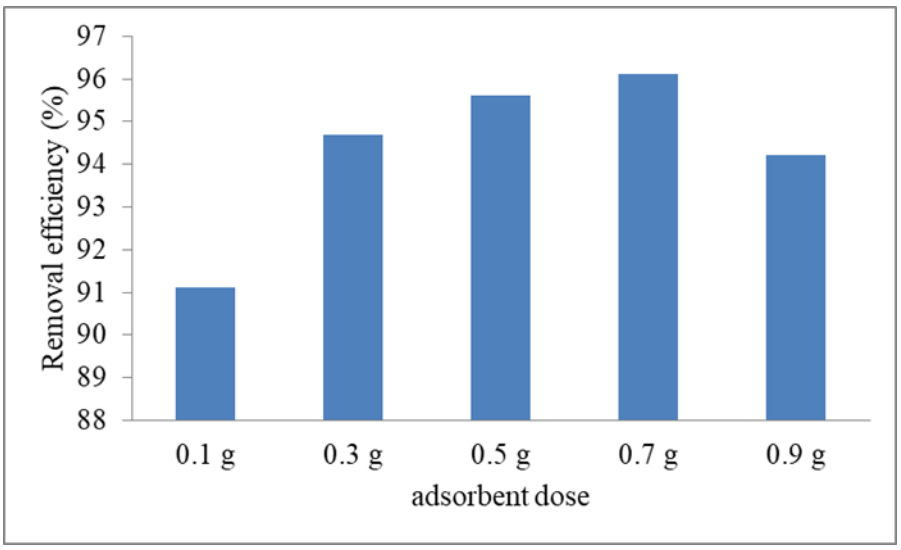

Figure 10: Effect of solution adsorbent doses on removal efficiency of fluoride ion

3.8.3. Determination of contact time

During adsorption process, determination of the effect of contact time is very important. The effect of contact time was determined by varying the contact time interval from 1 hr to 7 hr with 2 hr increments. The effect of contact time was carried out by keeping all parameters constant like initial concentration of fluoride ion solution 10 mg/L, volume of fluoride solution 50 mL, optimized pH 3, optimized adsorbent dose 0.7 g which have high removal efficiency and the solution was mixed at a speed of 150 rpm at room temperature. Figure 11 shows that a rapid fluoride removal was observed at the initial stage contact time until reaching equilibrium time with high removal efficiency. Figure 11 shows that the maximum removal efficiency of fluoride ion was achieved at contact time 3 hr which is 98 %. As contact time increases from 1 hr to 3 hr the removal efficiency of fluoride ion was increased. This is due to a high number of active sites at the initial stage lead to high diffusion of fluoride ion towards the adsorbent surface. But after the equilibrium time is reached the removal efficiency of fluoride was decreased. This is due to the saturation of the active sites and no enough additional active sites of adsorbent with increasing contact time.

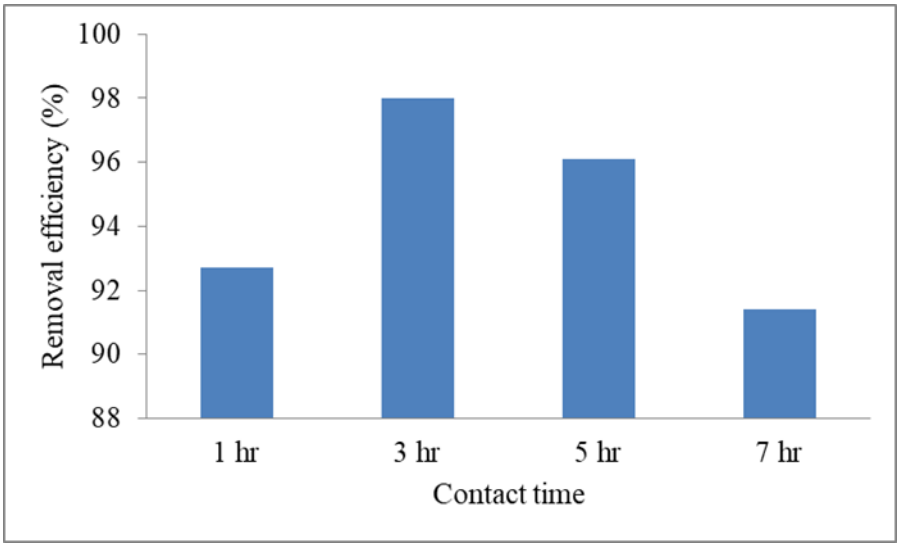

Figure 11: The result effect of contact time on removal efficiency of fluoride ion

3.8.4. Determination of initial concentration

The effect of initial concentration was determined by using the initial concentration interval from 10 mg/L to 25 mg/L with 5 increments. Investigating the effect of initial concentration on fluoride removal efficiency was carried out by keeping all parameters constant like volume of fluoride solution 50 mL, optimized adsorbent dosage 0.7 g, optimized pH 3, optimized contact time 3 hr which have high removal efficiency and shake the solution at speed of 150 rpm at room temperature. Figure 12 shows that the maximum removal efficiency of fluoride ion was achieved at initial concentration of 10 mg/L which is 98 %. There is high removal efficiency of fluoride at lower initial fluoride concentrations. This is because there is high active site of adsorbent surface at low concentration. From this study, the result indicates that, as the initial concentration of fluoride increases the removal efficiency of fluoride decreases. This is due to lack of sufficient surface area to accommodate more fluoride ions available in the solution. When the initial fluoride concentration increases for fixed mass of adsorbent there is no further removal of fluoride because all active site of adsorbent was occupied by fluoride at initial concentration.

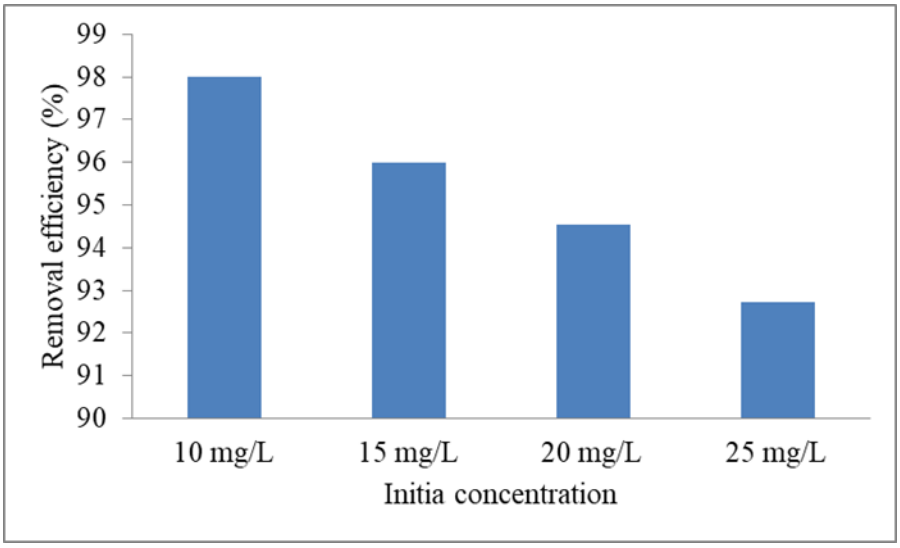

Figure 12: The result effect of initial concentration on removal of fluoride ion

3.9. Adsorption isotherms

Adsorption isotherm describes about the adsorbate adsorbed on adsorbent surface at equilibrium at constant temperature. It gives general idea about the effectiveness of the adsorbent in removing fluoride ions from water. Analysis of the isotherm data is very important because the isotherm describe equilibrium relationship between adsorbate and adsorbent for the adsorption process. For this study, the Langmuir adsorption isotherm model and Freundlich adsorption isotherm model were used to evaluate adsorption process. These two parameter models are simple and give a good description of experimental behavior in a large range of operating conditions. The two parameter models were determined from R^2 value.

3.9.1. Langmuir Adsorption Isotherm Model

The Langmuir adsorption isotherm model works based on the assumption of a monolayer and is dependent on the assumption that the adsorbent surface consists of active sites having a uniform energy of adsorption onto the surface of adsorbent.

Table 3: Langmuir's adsorption isotherm data

Initial Concentration (Co) in mg/L	Final Concentration (Ce) in mg/L	qe in mg/g	Ce/qe	LogCe	Logqe
10	0.2	0.70	0.286	- 0.699	- 0.1549
15	0.6	1.029	0.583	- 0.2218	0.0124
20	1.09	1.35	0.807	0.0374	0.1303
25	1.82	1.656	1.099	0.26	0.219

Adsorption capacity (qe) described the fluoride uptake capacity by unit mass of an adsorbent. From (Table 3) at low concentration (10 mg/L) the adsorption capacity is 0.7 mg/g, while at high concentration (25 mg/L) the adsorption capacity is 1.656 mg/g. This shows that as concentration increases adsorption capacity increases.

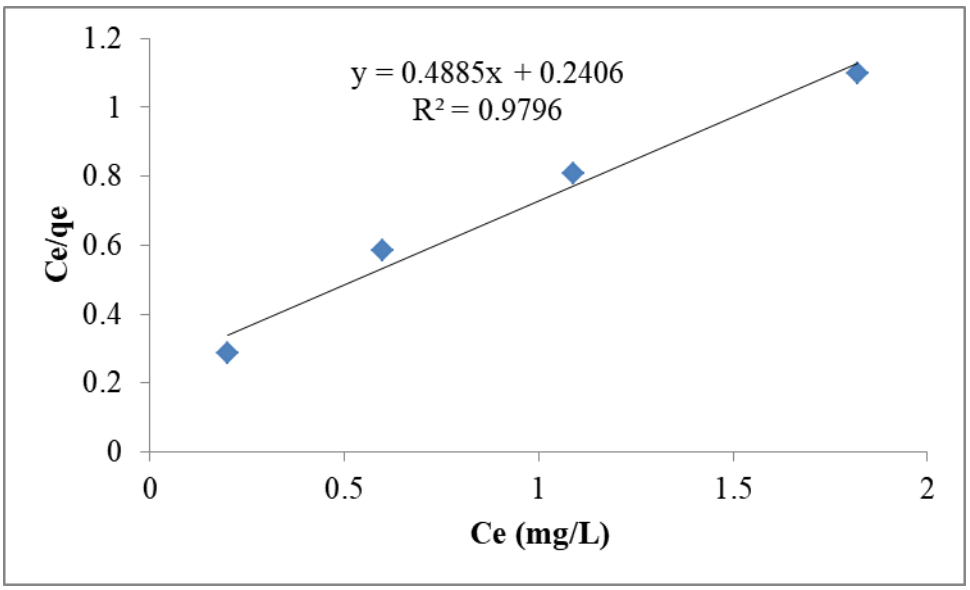

Figure 13: Linearized Langmuir adsorption isotherm concentration versus ratio of concentration to adsorption capacity for fluoride adsorption.

The Langmuir constants Q_{max} and b was determined from the slope of plotted graph and intercept of the plotted graph. That is $\frac{1}{bQ_{max}}$ is the slope and $\frac{1}{Q_{max}}$ is an intercept of the plot graph. From (Figure 13) the value of correlation coefficient (R^2), Langmuir constant related to maximum

adsorption capacity and rate of adsorption were calculated 0.9796, 4.2 mg/g and 0.49 L/mg, respectively. The result 4.2 mg/g of Q_{max} indicated that the maximum adsorption capacity for this adsorbent is 4.2 mg/g even when there was competition from the other commonly occurring anions. When the value of Langmuir constant (b) is relatively larger it indicates that there is a strong interaction between adsorbate and adsorbent while smaller value implies a weak interaction.The small result 0.49 L/mg rate of adsorption (b) indicated that there is weak interaction between adsorbate and adsorbent. The Langmuir isotherm can be explained by a dimensionless separation factor (RL) (Equation 9):

$$RL = \frac{1}{1 + bC_0} \quad \text{.......} \quad (9)$$

Where Co is the initial fluoride concentration and b is Langmuir constant.From the initial fluoride concentration the value of RL was calculated and found to be between 0 and 1 (0.1694 - 0.0755). The value of RL indicates the type of isotherm to be either irreversible (RL = 0), favorable (0 < RL< 1), unfavorable (RL > 1), linear (RL = 1). Depending on the RL values (shows in table 4) the adsorption of fluoride on the adsorbent under the experimental condition is favorable.

Table 4: The values of RL for fluoride adsorption by Fe doped HAp

Initial fluoride concentration (mg/L)	RL
10	0.1694
15	0.1197
20	0.0926
25	0.0755

3.9.2. Freundlich Adsorption Isotherm Model

The equilibrium data were analyzed using the Freundlich adsorption isotherm model. Freundlich-type adsorption is considered to be a multi-layer process in which the amount of adsorbed solute per unit adsorbent mass increases gradually. The Freundlich adsorption isotherm model equation takes into account repulsive interactions between adsorbed solute particles and also accounts for surface heterogeneities.

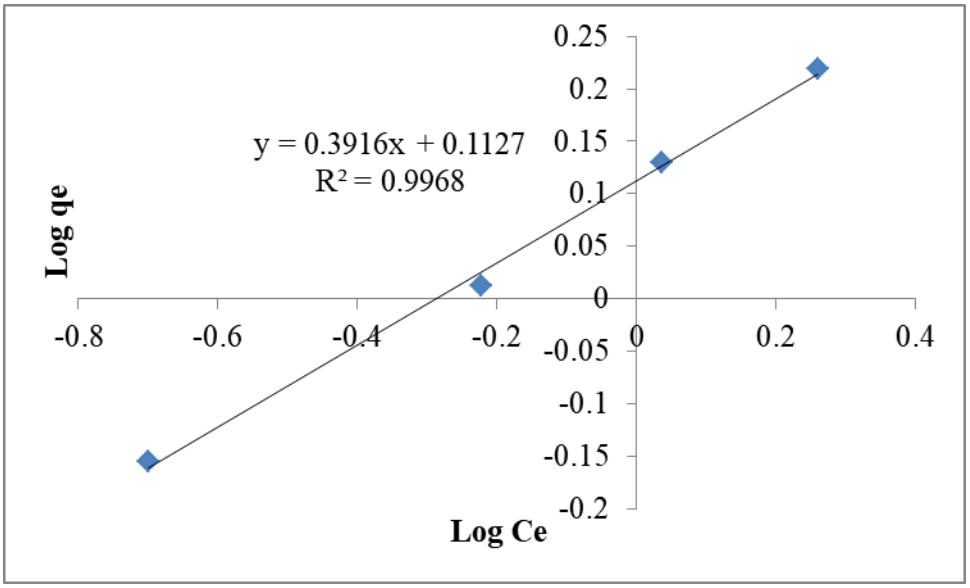

Figure 14: Freundlich adsorption isotherm log Ce versus log qe for fluoride adsorption.

The graph of log Ce versus log qe was plotted by using the result of log Ce and log qe in (Table 13).From (Figure 14) the value of Freundlich constant and adsorption capacity of the adsorbent was calculated. The value of K and n are calculated from the intercept and slope of the straight line of the plotted graph log Ce versus log qe.The value of 1/n is the slope and log K is an intercept of the plotted graph. The smaller value of K (1.3) represents a smaller adsorption capacity. The adsorption intensity of n values (2.55) lying between 1 and 10. Depending on n values it can be concluded that the adsorption of fluoride on the adsorbent under the experimental condition is favorable adsorption process. Correlation coefficients (R^2) values are used to determine whether the adsorption process follows Freundlich model or Langmuir isotherm model. Figures (13 and 14) show that the values of R^2 were 0.9796 and 0.9968 Langmuir isotherm model and Freundlich isotherm model, respectively. The R^2 of Freundlich isotherm model is greater than the Langmuir isotherm model. This indicated that the adsorption was multilayer adsorption on the structurally heterogeneous surface of the Fe doped HAp in the fluoride removal process. The R^2 value of Langmuir isotherm model is unacceptability model, because the correlation coefficient (R^2< 0.980). Adsorption data fitted well in linearized form of model equation (R^2> 0.980), which indicated the acceptability of the model [36].

3.10. Adsorption Kinetic Models

An investigation of the mechanism of adsorption process and its potential rate controlling steps that include mass transfer and chemical reaction processes, adsorption kinetic models are exploited to test the experimental data. Adsorption kinetic model is the measure of the adsorption uptake with respect to time at a constant concentration and is employed to measure the diffusion of adsorbate into on the adsorbent surface and in the pores of the adsorbent. The adsorption kinetic model experiments were carried out by using different contact times (1 hr, 3 hr, 5 hr and 7 hr) with other constant parameters like adsorbent dose 0.7 g and pH 3. Also the adsorption kinetics was studied with initial fluoride concentration 10, 15, 20 and 25 mg/L. From adsorption kinetic study experiments it is observed that a contact time of 3 hr was sufficient to achieve equilibrium of fluoride onto iron doped hydroxyapatite surface.

The kinetics study of fluoride adsorption was analyzed by Pseudo first order and pseudo second order models. Pseudo first order kinetic model described that the speed of occupation of adsorption sites is proportional to the number of unoccupied sites on the adsorbent surface. The pseudo second order kinetic model is based on the assumption that the rate limiting step is chemical adsorption and predicts the properties over the whole range of adsorption process.

Table 5: Parameters of pseudo first order and pseudo second order kinetics models for fluoride adsorption

Initial concentration mg/L	Contact time (min)	qe in mg/L	qt in mg/L	Log(qe-qt)	$\frac{t}{q_t}$
10	60	0.70	0.66	-1.398	90.91
15	180	1.029	0.7	- 0.4828	257.14
20	300	1.35	0.69	- 0.1804	434.78
25	420	1.656	0.65	0.0026	646.15

a). 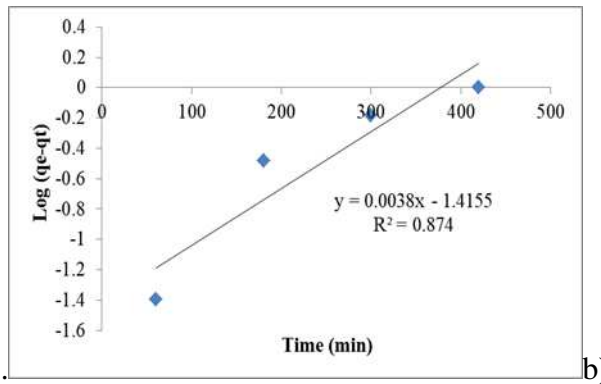

b). 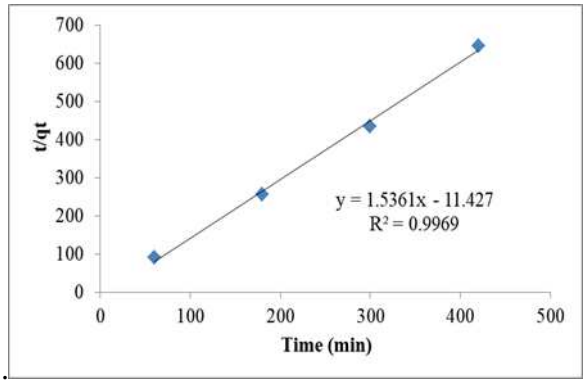

Figure 15: Result of kinetics model (a) pseudo first order kinetic model and (b) pseudo second order kinetic model

Table 6: Pseudo first order and pseudo-second-order kinetic constants model parameters

Pseudo first order					Pseudo second order				
Slope	Intercept	K_1 (min^{-1})	qe cal. (mg/g)	R^2	Slope	Intercept	K_2 (g/min mg)	qe cal.	R^2
0.0038	-1.4155	0.0088	0.0384	0.874	1.5361	-11.427	0.21	0.65	0.9969

Pseudo first order and pseudo second order constant (in table 6) were calculated using (Equations 6 and 7). Depending on correlation coefficient (R^2) the kinetics models were determined. Figures 15 shows that the values of correlation coefficient (R^2) were 0.874 and 0.9969 pseudo first order kinetics and pseudo second order kinetics, respectively. The R^2 of pseudo second order kinetics is greater than pseudo first order kinetics. This indicated that an experimental data of the present study best fits to the pseudo second order kinetics. Also the value of pseudo first order rate constant K_1 and the value of pseudo second order rate constant K_2 was described adsorption kinetics. The value of $K_1 < K_2$; this indicates that the higher energy sites had a much lower affinity for fluoride. Larger adsorption rate constant K_1 usually represents a quicker adsorption rate while larger values of adsorption rate constant K_2 represent a slower adsorption rate [37].

3.11. Defluoridation of Ground Water

The performance of Fe doped HAp defluoridation was evaluated by applying on groundwater. The fluoride concentration of the ground water was found to be 6.9 mg/L. The defluoridation of ground water were done by taking optimum batch adsorption parameters like pH adjusted at 3, adsorbent dosage 0.7 g, volume of treated ground water 50 mL, and shaking speed at 150 rpm for 3 hr at room temperature. After adsorption, the synthesized biomaterial powder removal efficiencies and adsorption capacity were calculated.The removal efficiency and adsorption capacity of fluoride from ground water by Fe doped HAp powder were 82.9 % and 0.41 mg/g, respectively. After adsorption, the pH was decreased from 8.2 to 6.9, this is due to the negative fluoride ions neutralized some positive charges on the adsorbent surface. The result of fluoride removal efficiency indicated that iron doped hydroxyapatite from the groundwater samples was lower than that of the synthetic replicated NaF solutions. The Tuch Dambali groundwater samples were taken from the Ethiopian Rift Valley contained high concentration of co-ions. The pH of the real Tuch Dambali groundwater samples was measured to be 8.2. This pH shows basic water solution. In basic solution, the presence of high concentration of HCO^{3-} and SO_4^{2-} ions interfere the uptake of fluoride ions by the adsorbents [38].

3.12. Regeneration and Desorption of Adsorbent

Regeneration is used to reuse the adsorbent after desorption process was occurred. Regeneration techniques are very important to evaluate the application of biomaterial, its duration time, reduce the cost of the process and decrease the amount of undesired wastes. The adsorption of fluoride can be attributed to electrostatic interactions between the surface charge of adsorbent and fluoride ions in the aqueous solution [39]. The mechanism (show in Equation 10 and 11), the interaction between the surface of Fe doped HAp and the F^- do not lead to a chemical reaction because it has been demonstrated that the adsorption of F^- on Fe doped HAp was reversible.

Desorption is the reverse process, that is release of the adsorbed adsorbate from the surface of adsorbent. Fluoride ion adsorbed on surface of hydroxyapatite was desorbed and released into solution by NaOH solution. In the determination of regeneration and desorption, the residual of adsorbent was washed and dispersed by using 1 N NaOH solution having pH of 13. This is because, with increasing pH, the fluoride ion captured in the hydroxyapatite structure was released into solution, exchanged by the hydroxide ion, an ionic substitution mechanism already

described in other studies [6, 39]. The use of NaOH solutions was better used for regeneration and desorption of HAp when compared to other compounds [40]. The OH^- remove the proton from adsorbent surface site and form water, the Na^+ remove F^- from adsorbent surface site and form NaF. The hydroxyapatite phase, the following reactions take place at elevated pH maintained during regeneration and desorption [41].

$$Ca_{(10-x)/2}Fe_{x/2}(PO_4)_3(OH) + F^- \rightarrow Ca_{(10-x)/2}Fe_{x/2}(PO_4)_3(OH) \equiv F^- \quad (10)$$

$$Ca_{(10-x)/2}Fe_{x/2}(PO_4)_3 OH_2^+ + F^- \rightarrow Ca_{(10-x)/2}Fe_{x/2}(PO_4)_3 OH_2^+ F^- \quad (11)$$

$$Ca_{(10-x)/2}Fe_{x/2}(PO_4)_3 OH_2^+ F^- + OH^- \rightarrow Ca_{(10-x)/2}Fe_{x/2}(PO_4)_3(OH) \equiv F^- + H_2O \quad (12)$$

$$Ca_{(10-x)/2}Fe_{x/2}(PO_4)_3(OH) \equiv F^- \rightarrow Ca_{(10-x)/2}Fe_{x/2}(PO_4)_3(OH) + F^- \quad (13)$$

Adsorption in (Equation 10) take place at higher pH, in abundance of OH^- ions, while adsorption in (Equation 11) take place at lower pH , in abundance of H^+ ions. (Equation 12 and 13) shows the mechanism of fluoride removal from surface site of adsorbent. The % adsorption efficiency and % desorption efficiency fluoride by NaOH solution were calculated using the following Equation 14 and 15:

$$\% \text{ adsorption capacity} = \left(\frac{C_o - C_f}{m}\right)V \quad (14)$$

$$\% \text{ desorption} = \frac{C_{des.}}{C_{ads.}} \times 100 \quad (15)$$

Where Co initial concentration (mg/L), Cf final concentration (mg/L), C_{des} concentration of fluoride desorbed (mg/L) and C_{ads} concentration of fluoride adsorbed (mg/L).

Five consecutive adsorption–desorption cycles were performed to study the regeneration and recyclability of the synthesized biomaterial. After five cycles, the fluoride desorption were 96.22 %, 95.72 %, 95.41 %, 95.2 % and 94.76 % respectively. After five cycles, the fluoride removal efficiency was 98 %, 91.1 %, 97.2 %, 82.5 %, and 80.2 % respectively.From these result the regeneration removal efficiency of fluoride, the fluoride removal was decreased. This is because the mass of residual adsorbent was decreased, while the volume of solution and concentration of fluoride in solution were constant in all five cycles. Another reason is the fluoride adsorbed on

adsorbent was not total desorbed.The fluoride removal was changed by small amount. Therefore, the synthesized adsorbent was suitable for regeneration and reusing.

3.13. Antibacterial Activity

Synthesized biomaterials were evaluated on antibacterial activity against gram negative E.coli bacteria and gram positive S. aureus bacteria. Contrimoxazole was taken as the standard (positive control) for all bacterial strains and DMSO was taken as negative control. Four different concentrations (3.73 mg/L, 7.5 mg/L, 15 mg/L and 30 mg/L) were prepared for studying the antibacterial activity. All concentration can be used on one plate for one bacteria species.

3.13.1. Antibacterial Activity of HAp

The evaluation of synthesized hydroxyapatite on antibacterial activity test against the E. coli bacteria and S.aureus bacteria were recorded in (Table 7).

Table 7: Antibacterial efficiency of HAp

Types of sample and organism			Diameter of Zone of inhibition observed at different concentration of samples in mm					
No	Types of sample	Types of bacteria	3.75 mg/mL (D)	7.5 mg/mL (C)	15 mg/mL (B)	30 mg/mL (A)	Contrimoxazole (+ ve)	DMSO (- ve)
1	HAp	E.Coli	9	10	11	11	21	6
		S.aureus	6.5	7	8	8	22	6

From (Table 7) the largest inhibition zones were recorded with 30 mg/ mL concentration gram negative bacteria E.coli (11 mm) and gram-positive bacteria S. aureus (8 mm). The lowest inhibition zones were recorded with 3.75 mg/ mL gram negative bacteria E.coli (9 mm) and gram-positive bacteria S. aureus (6.5 mm). At 3.75 mg/mL concentration the inhibition zone of negative control and the inhibition zone of gram-positive bacteria S. aureus had closely diameter. This shows that at lower concentration of pure HAp had low inhibition zone of S. aureus bacteria.

When synthesized HAp compared with standard drug (Contrimoxazole), Contrimoxazole have the greatest inhibition effect against both bacteria rather than synthesized HAp, the control solvents (DMSO) has no inhibition zone and showed no effect to the test solutions. Table 7 shows that the bacterial growth decreases as concentration of HAp increases. As it is shown in (Table 7) HAp is more inhibitory gram-negative bacteria E.coli than gram-positive bacteria S. aureus. This is due to the cell wall attributes differ between gram-negative E. coli and gram-positive S. aureus bacteria. E. coli has a relatively thin cell wall made of peptidoglycans while S. aureus has a relatively thick cell wall made of large amount of mucopeptides [42]. The permeability of Ca^{2+} ions of HAp is more in gram-negative bacteria due to thin cell walls. Ca^{2+} ions showed their effect on the oxygen consumed by the bacteria along with the production of free oxidative radicals that caused damage of cell membrane of the bacteria [43]. The Gram-positive S. aureus bacteria are less susceptible to Ca^{2+} ions than Gram-negative E. coli bacteria due to differences in their membrane structure and have thicker cell wall [42].

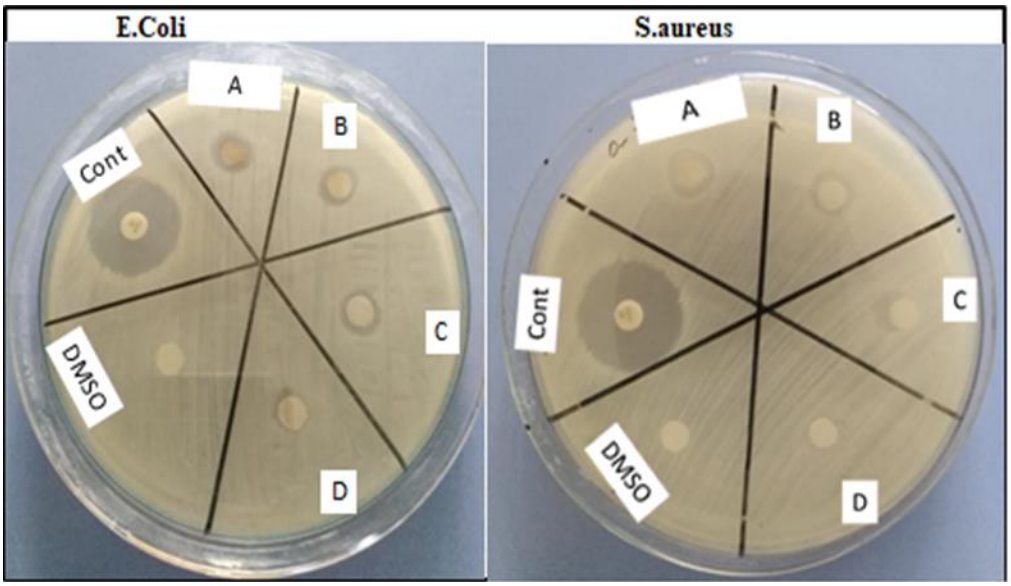

Figure 16: Antibacterial activity of hydroxyapatite at different concentrations against E.coli and S.aureus.

3.13.2. Antibacterial Activity of Fe doped HAp

Table 8: Antibacterial efficiency of Fe-HAp

Types of sample and organism			Diameter of Zone of inhibition observed at different concentration of samples in mm					
No	Types of sample	Types of bacteria	3.75 mg/mL (D)	7.5 mg/mL (C)	15 mg/mL (B)	30 mg/mL (A)	Contri-moxazole (+ ve)	DMSO (- ve)
1	HAp	E.Coli	7	9	10	11	21	6
		S. aureus	6	6	6	6	23	6

From (Table 8) the largest inhibition zones were recorded with 30 mg/ mL concentration against E.coli (11 mm) and the lowest inhibition zones were recorded with 3.75 mg/ mL against E.coli (7 mm). As concentration of Fe-HAp increases, the inhibition zone of E.Coli bacteria increases.

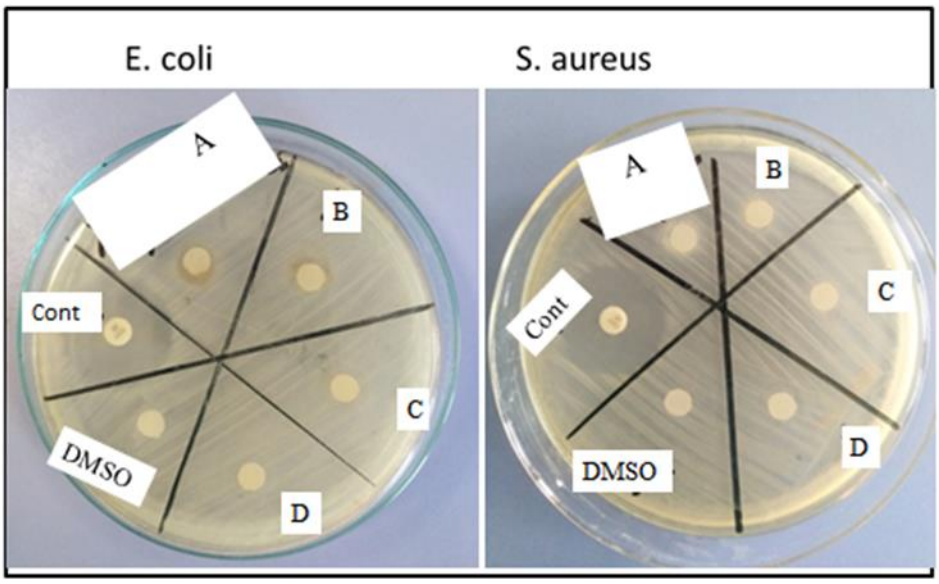

Figure 17: Antibacterial activity of iron doped hydroxyapatite at different concentration against E.coli and S.aureus

The inhibition zone reflects the bacteria sensibility to toxic agents so that the disinfectant-sensitive strains show large inhibition diameter and the resistant strains show a smaller or zero inhibition diameter. Figure 17 shows that at largest and lowest concentration of Fe-HAp no

inhibition zone against bacteria S. aureus was observed. The inhibition zone of negative control (DMSO) and inhibition zone of sample was equal in diameter. The thick cell wall of gram-positive bacteria S.aureus resists antibacterial agents. In generally, the synthesized HAp was more effective against bacteria strains than the synthesized Fe-HAp. Also the synthesized Fe doped HAp is effective antibacterial activity in gram negative bacteria than gram positive.

4. Conclusion

This study was investigated, the synthesis of Fe doped hydroxyapatite from commercial chemicals through the combustion method used for defluoridation of water by adsorption method and antibacterial activity by disc diffusion method. The Langmuir adsorption isotherm, Freundlich adsorption isotherm models, pseudo-first-order kinetics and pseudo-second-order kinetics models were used for the description of the adsorption equilibrium of fluoride. The adsorption data fitted well with the Freundlich adsorption isotherm models with a good correlation coefficient value which indicates multilayer adsorption on the heterogeneous adsorbent surface. The fluoride removal efficiency of HAp at pH 3, 95.6 % and at pH 7, 91.1 % as measured by fluoride ion selective electrode; it shows that the adsorption of fluoride is pH dependent. The synthesized adsorbent was applied to the ground water under optimum adsorption conditions (contact time 180 min, adsorbent dosage 0.7 g, pH 3, volume of solution 50 mL, at room temperature, and shaking speed 150 rpm, 6.9 mg/L of fluoride concentration of ground water and found to be effective with 82.9 % fluoride removal efficiency. The maximum adsorption capacity of synthesized Fe doped HAp was 4.2 mg/g. The maximum inhibition zone of gram-negative bacterial strains E. coli 11 mm was recorded for Fe doped HAp. But there is no inhibition zone of gram-positive bacterial strains S.aureus was recorded for Fe doped HAp. In generally, it concluded that Fe doped HAp can be employed for fluoride removal from groundwater rather than antibacterial activities.

Declarations

Ethics approval and consent to participate

Not applicable.

Consent for publication

All authors of the manuscript agreed to publication

Acknowledgement

The authors would like to thank Adama Science and Technology University financial and material support and Oromo Self Help Organization (OSHO) Fluoride Removal Technology Center for providing laboratory facilities.

Authors' contributions

Abebe Awulew conducted the experiments, analysis the data, and wrote the manuscript, Dereje Tsegaye supervised the work and wrote the manuscript, and Enyew Amare initiated the research work, supervised work and reviewed the manuscript.

Funding: This work was supported by Adama Science and Technology University.

Conflicts of Interest: There are no conflicts to declare.

Data availability statement

All data that support the outcomes of this research study are included within the article.

Reference

1. Dhillon, A., Nair, M., Bhargava, S. K., & Kumar, D. (2015). Excellent fluoride decontamination and antibacterial efficacy of Fe-Ca-Zr hybrid metal oxide nanomaterial. J Colloid and Interf Sci 457:289–297

2. Ergun, E., Tor, A., Cengeloglu, Y., &Kocak, I. (2008). Electrodialytic removal of fluoride from water: Effects of process parameters and accompanying anions. Separation and Purification Technology 64:147–153

3. Jiménez-Reyes, M., & Solache-Ríos, M. (2010). Sorption behavior of fluoride ions from aqueous solutions by hydroxyapatite. J Hazardous Materias 180: 297–302.

4. Kumar, S., & Jain, S. (2013). History, introduction, and kinetics of ion exchange materials. J Chem 13:957647

5. Mourabet, M., Rhilassi, A. El, Boujaady, H. El, Hamri, R. El, & Taitai, A, Removal of fluoride from aqueous solution by adsorption on hydroxyapatite (HAp) using response surface methodology. J Saudi Chemical Society (2012)

6. Sundaram, C. S., Viswanathan, N., & Meenakshi, S. (2008). Defluoridation chemistry of synthetic hydroxyapatite at nano scale : Equilibrium and kinetic studies. J Hazardous Materias 155:206–215

7. Sternitzke, V., Kaegi, R., Audinot, J. N., Lewin, E., Hering, J. G., & Johnson, C. A. (2012). Uptake of fluoride from aqueous solution on nano-sized hydroxyapatite: Examination of a fluoridated surface layer. ACS Environ. Sci. Technol. 46:802–809.

8. Kanno, C. M., Sanders, R. L., Flynn, S. M., Lessard, G., & Myneni, S. C. B. (2014). Novel Apatite-Based Sorbent for Defluoridation: Synthesis and Sorption Characteristics of Nano-micro-crystalline Hydroxyapatite- Coated-Limestone. ACS Environ. Sci. Technol. 48:5798−5807

9. Xia Y, Huang X, LiW, Zhang Y, Li Z, Facile Defluoridation of Drinking Water by Forming Shell@Fluorapatite Nanoarray during Boiling Egg Shell, J Hazardous Materials (2018)

10. D. Mehta, P. Mondal, V. Kumar Saharan, S. George, Synthesis of Hydroxyapatite Nanorods for application in water defluoridation and optimization of process variables: Advantage of ultrasonication with precipitation method over conventional method, Ultrasonics Sonochemistry (2016)

11. Zaman, S. U., Khaliq, M., Zaman, U., & Muhammad, N. (2020). Overview of hydroxyapatite; composition, structure, synthesis methods and its biomedical uses. Biomedical Letters 6:84–99

12. Méndez-lozano, N., Velázquez-castillo, R., Rivera-muñoz, E. M., Bucio-galindo, L., Mondragón-galicia, G., Manzano-ramírez, A., Ángel, M., & Apátiga-castro, L. M,

Crystal growth and structural analysis of hydroxyapatite nanofibers synthesized by the hydrothermal microwave-assisted method. Ceramics International (2016)

13. Batista, H. A., Silva, F. N., Lisboa, H. M., & Costa, A. C. F. M, Modeling and optimization of combustion synthesis for hydroxyapatite production. Ceramics International (2020)

14. Cahyaningrum, S. E., Herdyastuty, N., Devina, B., &Supangat, D. (2018). Synthesis and Characterization of Hydroxyapatite Powder by Wet Precipitation Method. IOP Conf. Ser.: Mater. Sci. Eng. 299: 012039

15. Cao, L. Y., Zhang, C. B., & Huang, J. F. (2005). Synthesis of hydroxyapatite nanoparticles in ultrasonic precipitation. Ceramics International 31:1041–1044.

16. Yuan, Y., Liu, C., Zhang, Y., & Shan, X. (2008). Sol – gel auto-combustion synthesis of hydroxyapatite nanotubes array in porous alumina template. Mater Chem Phys112:275–280

17. Govindaraj, D., & Rajan, M. (2016). Synthesis and Spectral Characterization of Novel nano-Hydroxyapatite from Moringa oleifera Leaves. Materials Today: Proceedings 3: 2394–2398

18. Koumoulidis, G. C., Katsoulidis, A. P., Ladavos, A. K., Pomonis, P. J., Trapalis, C. C., Sdoukos, A. T., & Vaimakis, T. C. (2003). Preparation of hydroxyapatite via micro emulsion route. J Colloid and Interf Sci 259: 254–260

19. Pramanik, S., Agarwal, A. K., Rai, K. N., & Garg, A. (2007). Development of high strength hydroxyapatite by solid-state sintering process. Ceramics International 33: 419–426

20. Khandelwal, H. and Prakash, S. (2016) Synthesis and Characterization of Hydroxyapatite Powder by Eggshell. J Minerals and Materials Characterization and Engineering 4:119-126

21. Malla, K. P., Regmi, S., Nepal, A., Bhattarai, S., Yadav, R. J., Sakurai, S., & Adhikari, R, Extraction and Characterization of Novel Natural Hydroxyapatite Bioceramic by Thermal Decomposition of Waste Ostrich Bone. Int. J Biomater 10: 1690178

22. Han, Y., Li, S., Wang, X., & Chen, X. (2004). Synthesis and sintering of nanocrystalline hydroxyapatite powders by citric acid sol-gel combustion method. Materials Research Bulletin 39:25–32

23. Ismail, N. F., Hamzah, S., Razali, N. A., Yussof, W. M. H. W., Ali, N., & Mohammad, A. W. (2019). Preparation and characterization of hydroxyapatite extracted from fish scale waste for the removal of gallic acid as inhibitor in biofuel production. Malaysian J Analytical Sci 23:938–949

24. Shi, P., Liu, M., Fan, F., Yu, C., Lu, W., & Du, M. (2018). Characterization of natural hydroxyapatite originated from fish bone and its biocompatibility with osteoblasts. Mater Sci Eng C 90: 706–712

25. Hadagalli, K., Shenoy, S., Shakya, K. R., Manjunath, G., Tarafder, K., Mandal, S., & Basu, B. (2021). Effect of Fe^{3+} substitution on the structural modification and band structure modulated UV absorption of hydroxyapatite. Int. J Appl Ceramic Technol 18: 332–344

26. Rock, C., & Rivera, B, Water Quality, E. coli and Your Health. College of Agriculture and Life Science (2014)

27. Jose, S., Senthilkumar, M., Elayaraja, K., Haris, M., George, A., Raj, A. D., Sundaram, S. J., Bashir, A. K. H., Maaza, M., Kaviyarasu, K., West, S., Province, W. C., & Africa, S.(2021). Preparation and characterization of Fe doped n -hydroxyapatite for biomedical application. Surfaces and Interfaces 25: 101185

28. Fan, X., Parker, D. J., & Smith, M. D. (2003). Adsorption kinetics of fluoride on low cost materials. Water Research 37: 4929–4937

29. Dadi, R., Azouani, R., Traore, M., Mielcarek, C., & Kanaev, A, Antibacterial activity of ZnO and CuO nanoparticles against gram positive and gram negative strains. Mater Sci Eng C (2019)

30. Kabir, S. F., Ahmed, S., Mustafa, A. I., Ahsan, M., & Islam, S. (2012). Synthesis and Characterization of Fe-doped Hydroxyapatite. Bangladesh J. Sci. Ind. Res. 47: 1-8

31. Kaygili, O., Dorozhkin, S. V., Ates, T., Al-Ghamdi, A. A., & Yakuphanoglu, F. (2014). Dielectric properties of Fe doped hydroxyapatite prepared by sol-gel method. Ceramics International 40: 9395–9402

32. Goldberg, M. A. (2021) Mesoporous iron (iii)-doped hydroxyapatite nanopowders obtained via iron oxalate. Nanomaterials 11:811

33. Singh, B. (2018). Biomaterials Enhanced dielectric constant and structural transformation in Fe-doped hydroxyapatite synthesized by wet chemical method. J Mater Sci

34. Dardouri, M., Borges, J. P., & Omrani, A. D. (2017). Tailoring the morphology of hydroxyapatite particles using a simple solvothermal route. Ceramics International 43:3784–3791

35. Chowdhury, S., Mishra, R., Saha, P., &Kushwaha, P. (2011). Adsorption thermodynamics, kinetics and isosteric heat of adsorption of malachite green onto chemically modified rice husk. Desalination 265:159–168

36. Kanaujia, S., Singh, B., & Singh, S. K. (2015). Removal of Fluoride from Groundwater by Carbonised Punica granatum Carbon ("CPGC") Bio-Adsorbent. J Geosci. Environ. Protection 3: 1-9

37. Getachew, T., Hussen, A., &Rao, V. M. (2015). Defluoridation of water by activated carbon prepared from banana (Musa paradisiaca) peel and coffee (Coffea arabica) husk. Int. J Environ Sci Technol 12:1857–1866

38. Habuda-Stanić, M., Ravančić, M., & Flanagan, A. (2014). A Review on Adsorption of Fluoride from Aqueous Solution. Materials 7: 6317–6366

39. Medellin-castillo, N. A., Leyva-ramos, R., Padilla-ortega, E., & Perez, R. O. (2014). Adsorption capacity of bone chars for removing fluoride from water solution. Role of hydroxyapatite content adsorption mechanism and competing anions. J Ind Eng Chem 8: 1835

40. A.K, K., T. K, K., S. M, K., & C. K, C. (2014). Efficiency of various sodium solutions in regeneration of fluoride saturated bone char for de-fluoridation. IOSR J Environ Sci Toxicology and Food Technol 8:10–16

41. Sarkar, G. T. A. T. S. (2015). Enhanced fluoride removal by hydroxyapatite-modified activated alumina. Int. J Environ. Sci. and Technol. 12:2809–2818

42. Ragab, H. S., Ibrahim, F. A., Abdallah, F., A. (2014). Synthesis and In Vitro Antibacterial Properties of Hydroxyapatite Nanoparticles. IOSR J Pharmacy and Biological Sci 9:77–85

43. Tejaswini, T., Keerthana, M., Vidyavathi, M., & Kumar, R. V. S. (2020). Design and evaluation of atorvastatin- loaded chitosan-hydroxyapatite composite bioscaffolds for wound-healing activity. Future J Pharmaceutical Sci. 6:111